Desalination and Water Treatment
www.deswater.com

doi:10.5004/dwt.2017.0457

59 (2017) 114–122
January

Inhibition of calcium scales by a fluorescent-tagged and polyether-based polycarboxylate scale inhibitor for cooling water systems

Ao Zhang[a], Yuming Zhou[a,*], Qingzhao Yao[a,*], Tiantian Wang[a], Jun Li[a], Yiyi Chen[a], Jie Pan[a], Shuang Liang[a], Qiuli Nan[b], Mingjue Zhang[b], Wei Sun[c], Wendao Wu[c], Jin Hou[d]

[a]*School of Chemistry and Chemical Engineering, Southeast University, Nanjing 211189, China, Tel. +86 25 52090617; emails: 220142382@seu.edu.cn (A. Zhang), ymzhou@seu.edu.cn (Y. Zhou), 101006377@seu.edu.cn (Q. Yao), 1439127031@qq.com (T. Wang), 1543107327@qq.com (J. Li), 838331357@qq.com (Y. Chen), 769809870@qq.com (J. Pan), 769809870@qq.com (S. Liang)*
[b]*Cheng Xian College, Southeast University, Nanjing 211189, China, Tel. +86 13770899929; email: 53212651@qq.com (Q. Nan); Tel. +86 13805195819; email: 489354839@qq.com (M. Zhang)*
[c]*Jianghai Environmental Protection Co., Ltd, Changzhou, Jiangsu, 213116, China, Tel. +86 25 52090617; emails: leojhhg@sina.com (W. Sun), 13887303@qq.com (W. Wu)*
[d]*Nantong Entry-exit Inspection and Quarantine Bureau, Nantong 226000, China, Tel. +86 0513-3533522; email: houjinnt@aliyun.com (J. Hou)*

Received 24 April 2016; Accepted 23 June 2016

ABSTRACT

To inhibit the carbonate and sulfate precipitations of calcium in cooling water systems, a water-soluble copolymer, acrylic acid-oxalic acid-methallyl methoxy polyethylene glycol-8-vinylbenzyloxy-1, 3, 6-pyrene trisulfonic acid trisodium salt (AA-HPEZ-VPTA) was synthesized. Structures of comonomer were carried out by FT-IR and ^{1}H-NMR. The novel inhibitor's ability to control calcium scales was better than current commercial inhibitors (PAA, PESA, HPMA), with about 92.1% for $CaCO_3$ and 98.9% for $CaSO_4$ at levels of 8 and 4 mg/L, respectively. The effect on formation of calcium scales was investigated with combination of scanning electronic microscopy and X-ray powder diffraction analysis. The correlation coefficient r of inhibitor's is 0.9971. AA-HPEZ-VPTA can be used as an effective fluorescent-tagged scales inhibitor for cooling water systems.

Keywords: Fluorescent tagged; Copolymerization; Non-phosphate; Scale inhibitor

1. Introduction

Circulating cooling water systems are the most commonly industrial waste heat rejection systems [1]. However, water used in the cooling water systems usually contains scale-forming ions such as Ca^{2+}, HCO_3^- and SO_4^{2-} [2]. Scale-forming ions solubility limits could be easily exceeded because of the evaporation of water, which leads to the deposition of mineral scales on the equipment surfaces [3]. The scales formation poses great problems from both economic and technical points of view, reducing heat transfer efficiency and causing damage of the water piping [4,5].

Many effective measures have been widely used to mitigate the mineral scaling problems [6,7]. The most common and effective method to control or prevent scale formation is to add scale inhibitors [8]. There are many classes of polymers used as scale inhibitors to control scale formation. Most of them are water-soluble polymers with several functional groups such as phosphonate, carboxylate, and sulfonate. Poly-phosphonate type scale inhibitors are most widely used and effective to inhibit calcium scales growth [9]. Unfortunately, they can easily lead to the formation of orthophosphate because of hydrolysis or decomposition [10,11], and orthophosphate can react with calcium ions to form relatively insoluble calcium phosphate scale [12]. In addition, orthophosphate is a potential nutrient for algae.

*Corresponding authors.

As a result, the current trend for inhibitor usage towards more environmentally green inhibitors such as poly aspartic acid and anhydride [13].

The concentration of inhibitors used in the cooling water systems should be controlled in a prescribed range to ensure its best efficiency [14]. In general practice, the concentration of water treatment agent in cooling water can be measured using analytical methods [15]. Compared to other analytical methods like potentiometric and spectrometric, fluorescence method is more accurate and efficient for the concentration determination, and most of the fluorescent tracers are available at low cost, and are environmentally acceptable [16,17]. Currently, preparation of fluorescent polymers scale inhibitors have two methods [18]. One is the copolymerization of fluorescence monomer with other monomers; the other method is chemical modification of polymers through fluorescent groups. Literature shows that fluorescent scale inhibitors prepared by the method of chemical modification in dilute aqueous or mixed solvent systems exhibit poor stability [19]. Moriarty performed 8- vinylbenzyloxy -1, 3, 6-pyrene trisulfonic acid trisodium salt (VPTA) fluorescent monomers, and the hydrophilic of VPTA is strong because of containing three sulfoacid hydrophilic groups [20].

Compared to allyloxy polyethoxy ether (APEG), methallyl methoxy polyethylene glycol (HPEG) has a higher polymerization activity [21]. In recent years, various scale inhibitors based on APEG to control calcium scale depositions have been prepared by our group [22–25]. However, there is no report of scale inhibitor synthesized by HPEG used in cooling water systems. Especially, the influence of solution's pH on fluorescence intensity has never been studied in our previous work.

According to all these information, the aim of this study is to synthesize a green and fluorescent-tagged scales inhibitor. We use acrylic acid, oxalic acid-allypolyethoxy carboxylate (HPEZ) and VPTA to Synthesize PAHV (poly (AA-HPEZ-VPTA)) by radical polymerization. The relation between the concentration and fluorescence intensity of polymer was studied. Then, the effect of solution's pH on the fluorescence properties of PAHV was also investigated.

2. Experimental

2.1. Materials

8-Hydroxy-1, 3, 6-pyrene trisulfonic acid trisodium salt (pyranine) and 4-Vinylbenyl chloride (VBC) were purchased from energy Chemical (Shanghai, China). Methallyl methoxy polyethylene glycol (HPEG, 300 M_w), poly (acrylic acid) (PAA, 1800 M_w), poly (epoxy succinic acid) (PESA, 1500 M_w), and hydrolytic poly (maleic anhydride) (HPMA, 600 M_w) were obtained from Jianghai Reagent (Changzhou, Jiangsu, China). All other reagents, purchased from Zhongdong Chemical Reagent (Nanjing, Jiangsu, China), were analytical reagent grade and were used without further purification. Distilled water was used for all the studies.

2.2. Preparation of HPEZ, VPTA and PAHV

The synthesis procedure of HPEZ is shown in Fig. 1. HPEZ was synthesized from methallyl methoxy polyethylene glycol (HPEG) and oxalic acid at 80°C under nitrogen atmosphere for 4.0 h.

8-Vinylbenzyloxy-1,3,6-pyrene trisulfonic acid trisodium salt (VPTA) was synthesized according to Moriarty [20]. The product was a light yellow powder. The synthesis of VPTA from pyranine and 4-Vinylbenzyl chloride is shown in Fig. 2.

The synthesis procedure of PAHV from AA, HPEZ, and VPTA is shown in Fig. 3. VPTA was copolymerized with HPEZ and AA in aqueous medium. The copolymerization reaction was carried out in a 250 mL five-neck round-bottom flask with a mechanical stirrer, thermometer. 0.5 mole AA and 30 mL distilled water were mixed stirring continuously under nitrogen atmosphere. A definite proportion of HPEZ and VPTA were added in 20 mL distilled water and heated to the reaction temperature 70°C about 1.0 h. In fixed conditions, the initiator ammonium persulfate was dropped at a certain flow rate for more than 1.5 h. And then, the reactant was heated with stirring at 80°C for 2.0 h under nitrogen atmosphere. The polymer was separated by a large volume of acetone. The insoluble product was filtered, collected, and extracted in a soxhlet extractor for 10.0 h to remove the extra AA and HPEZ. The crude product was dried in a vacuum oven until constant weight, and then re-crystallized

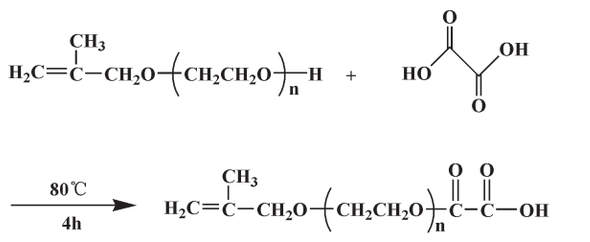

Fig. 1. Preparation of HPEZ.

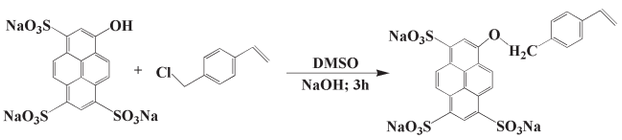

Fig. 2. Preparation of VPTA.

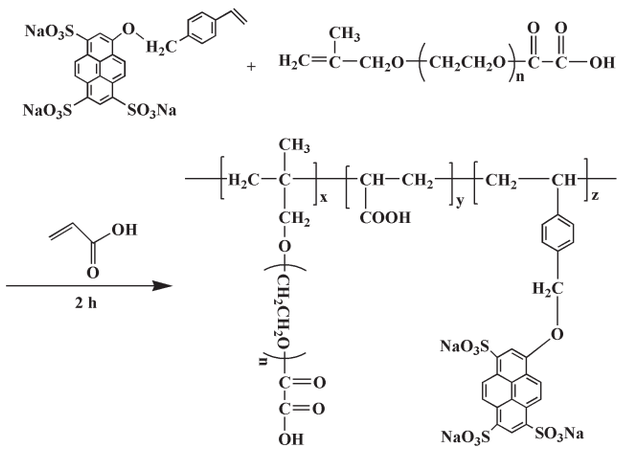

Fig. 3. Preparation of PAHV.

in water–acetone mixture (3:7 V/V) to remove the unused VPTA and gain PAHV as a light yellow solid.

2.3. Characterization

The samples were analyzed using a FT-IR spectroscopy (VECTOR-22, Bruker Co., Germany) in the region of 4,000–500 cm^{-1}. Structures of VPTA, HPEZ, and PAHV were also explored by a Bruker NMR analyzer (AVANCE AV-500, Bruker, Switzerland) operating at 500 MHz. X-ray diffraction (XRD) patterns of the $CaCO_3$ and $CaSO_4$ crystals were recorded on a Rigaku D/max 2,400 X-ray powder diffractometer with CuKα (λ = 1.5406) radiation (40 kV, 120 mA). The shape of $CaCO_3$ and $CaSO_4$ scale were observed with a Scanning electron microscopy (SEM) images were recorded using a field emission scanning electron microscope (S-3400 N HITECH). Fluorescence measurements were carried out on a luminescence spectrometry (LS-55, Perkin-Elmer, UK) with a xenon lamp as a light.

2.4. Static scale inhibition methods

The ability of the PAHV copolymer to inhibit calcium carbonate scale was compared with the free inhibitor in flask tests and all inhibitor dosages given below are on a basis of dried conditions [9]. The experiment was carried out in artificial cooling water which was prepared by a mixing aqueous solution of two soluble salts $NaHCO_3$ and $CaCl_2$. Two concentrations of Ca^{2+} and HCO_3^- were 480 and 1,464 mg/L, respectively. Tests of the inhibitors were carried out using supersaturated solutions of $CaCO_3$ at 80°C, the pH value of solution was held about 9 adjusting by borax buffer solution. According to the national standard of People's Republic of China (GB/T 16632–2008), every inhibition test was carried out in a 500 mL flask immersed in a temperature controlled bath for 10 h. Precipitation of $CaCO_3$ was monitored by analyzing aliquots of the filtered solution for Ca^{2+} ions using EDTA complexometry as specified in code GB/T 15452–2009. At the end point of titration, the color of the solution changed from purple into light blue using calcon carboxylic acid indicator. Inhibitor efficiency was calculated from the following equation [26]:

$$\text{Inhibition } (\%) = \frac{(Ca^{2+})_1 - (Ca^{2+})_0}{(Ca^{2+})_2 - (Ca^{2+})_0} \times 100\% \quad (1)$$

where $(Ca^{2+})_1$ = Ca^{2+} concentration of inhibited sample; $(Ca^{2+})_0$ = Ca^{2+} concentration of uninhibited sample; $(Ca^{2+})_2$ = initial Ca^{2+} concentration.

Procedure of calcium sulfate inhibition test was also carried out similarly to calcium carbonate precipitation experiments according to the national standard of P.R. China concerning the code for the design of industrial oilfield-water treatment (SY/T 5673–93). Calcium sulfate precipitation was studied in different artificial cooling water which was prepared by dissolving a certain quantity of $CaCl_2$ and Na_2SO_4 in deionized water. Two concentrations of Ca^{2+} and SO_4^{2-} were 6,800 and 7,100 mg/L, respectively. The pH of the calcium sulfate solutions were adjusted to 7.0 using sodium hydroxide and hydrochloric acid. The artificial cooling water containing different doses of the PAHV was at 70°C for 6.0 h in a water bath. The determination of Ca^{2+} was done by exactly same process. The inhibition efficiency of PAHV against calcium sulfate scale was calculated as Eq. (1).

2.5. Excitation and emission wavelength measurement of VPTA and PAHV

Excitation and emission wavelengths of VPTA and PAHV were all measured at β_{ex} = 402 nm (5 nm slid width) and β_{em} = 429 nm (5 nm slid width), respectively. About 4×10^{-7} mol/L VPTA distilled water solution was prepared. PAHV was dissolve in quantum sufficient distilled water and the concentration of VPTA in PAHV solution is also 4×10^{-7} mol/L.

2.6. Detection of PAHV fluorescent intensity with different concentration

Using inert fluorescent tracers and on-line fluorometer provides accurate control of treatment dosage and immediate response to change dosage of inhibitor. A series of different concentration of PAHV samples (1, 2, 3, 4, 5, 6, 7, 8 and 9 mg/L) were prepared into aqueous solution samples to estimate fluorescent intensity response to polymer's concentration.

2.7. Effect of pH on scale inhibitior fluorescent intensity

About 3 mg/L PAHV was prepared to investigate the changes of the fluorescent properties of PAHV in a phosphate buffer solvent at different pH values. The pH of the fluorescent scale inhibitor solutions were adjusted from 5 to 12 using phosphate buffered saline.

3. Results and discussion

3.1. FT-IR measurements

The FT-IR spectrum of VPTA is exhibited in Fig. 4. VPTA (FT-IR, cm^{-1}): 660–870 (C–H plane deformation vibration of aromatic compound), 1,008 (C–H plane deformation vibration of C = CH_2), 1,050 (alkyl oxide characteristic absorption of VPTA), 1,270 (fragrant ether characteristic absorption), 1,450–1,507 (aromatic compound absorption band), 1,642 (C=C stretching vibration), 3,450 (O–H stretching vibration). The two characteristic vibration bands of 1,270 and 1,050 cm^{-1} exist to prove the monomer structure which includes alkyl aryl ether.

The FT-IR spectra of HPEG (a), HPEZ (b) and PAHV (c) are exhibited in Fig. 5. The 1,743 cm^{-1} strong intensity absorption peak (–C=O) in curve (b) clearly reveals that HPEZ has been synthesized successfully. The fact that the (–C=C–) stretching vibration at 1,642 cm^{-1} appears in curve (b) but disappears completely in curve (c) reveals that radical polymerization between AA, HPEZ, and VPTA has happened [27].

3.2. ^{1}H-NMR studies

^{1}H-NMR images of pyranine (PY) and VPTA are shown in Fig. 6. The ^{1}H-NMR data were acquired as the following and the chemical molecule structures were deduced as expected.

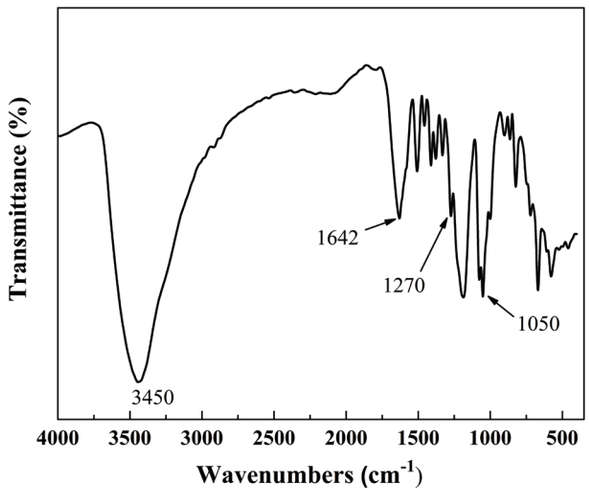

Fig. 4. FT-IR spectrum of VPTA.

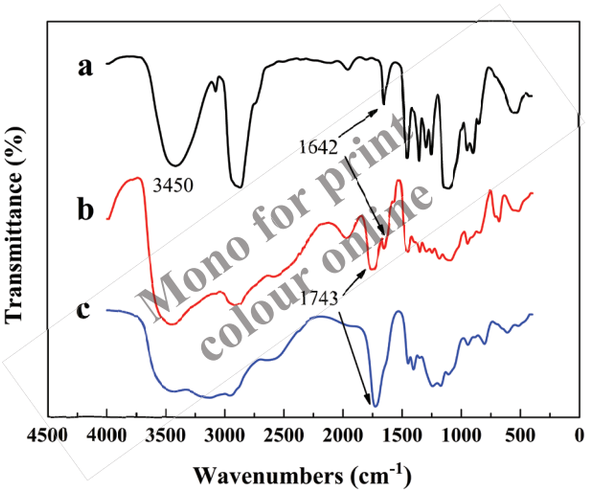

Fig. 5. FT-IR spectra of (a) HPEG, (b) HPEZ and (c) PAHV.

PY (a) [$(CD_3)_2SO$, δ ppm]: 2.40–2.60 (solvent residual peak of $(CD_3)_2SO$), 8.10–9.15 (six protons of benzene ring in PY), 10.64 (–OH, active hydrogen in PY).

VPTA (b) [$(CD_3)_2SO$, δ ppm]: (2.40–2.60 solvent residual peak of $(CD_3)_2SO$), 5.27–5.30 and 5.85–6.81 (CH_2=CH–, vinyl protons), 5.50–5.53 (methylene protons), 7.55–7.65 (four protons of benzene ring in VPTA), 8.10–9.15 (six protons of benzene ring in VPTA).

VPTA has three different types of protons, the vinyl protons, methylene protons and benzene ring protons corresponding position in three absorption peaks, and the Fig. 6(b) shows the integral structure consistent with the area. The complete disappearance of δ 10.63–10.65 ppm active hydrogen (–OH) in (a) proves that –OH in VPTA has been entirely replaced by p-methyl styrene group. It certifies that the product has expected structure.

^{1}H-NMR images of HPEG (a), HPEZ (b), and PAHV (c) are shown in Fig. 7. The ^{1}H-NMR data were acquired as the following and the chemical molecule structures were deduced as expected.

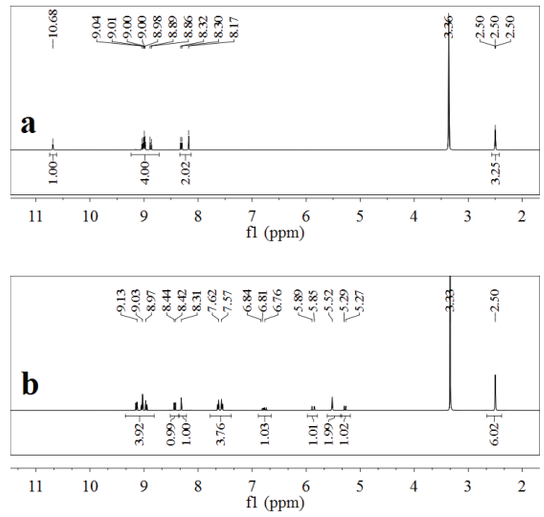

Fig. 6. ^{1}H-NMR spectra of PY (a) and VPTA (b).

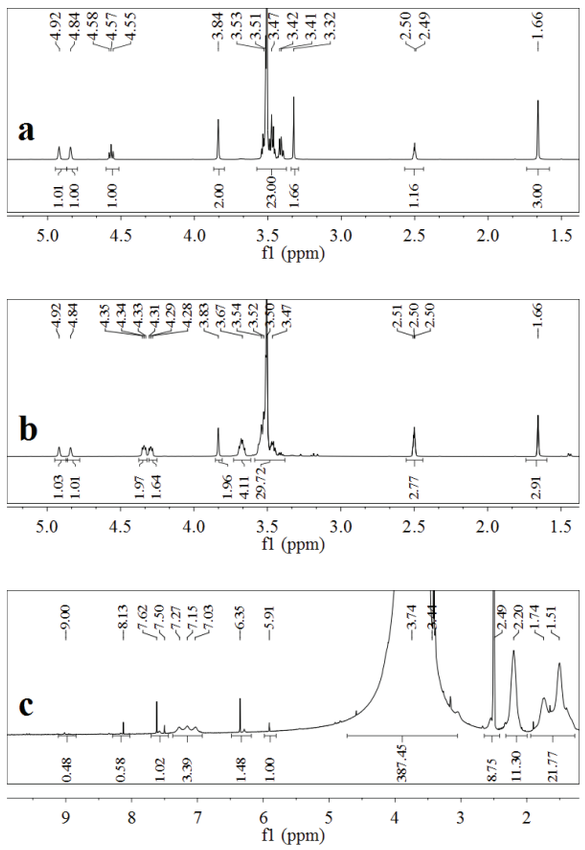

Fig. 7. ^{1}H-NMR spectra of HPEG (a), HPEZ (b) and PAHV (c).

HPEG (a) [$(CD_3)_2SO$, δ ppm]: 2.50 (solvent residual peak of $(CD_3)_2SO$), 3.30–3.60 (–OCH_2CH_2–, ether groups), 1.66 and 3.82–4.95 (CH_2 = C (CH_3)–CH_2–, propenyl protons), and 4.50–4.60 (–OH, active hydrogen in HPEG).

HPEZ (b) [$(CD_3)_2SO$, δ ppm]: 2.50 (solvent residual peak of $(CD_3)_2SO$), 3.40–4.32 (–OCH_2CH_2–, ether groups), 1.66 and 4.33–4.95 (CH_2 = C (CH_3)–CH_2–, methyl allyl protons).

PAHV (c) [$(CD_3)_2SO$, δ ppm]: (2.50 solvent residual peak of $(CD_3)_2SO$), 1.45–1.78 (–CH_3, methyl proton) and 3.30–4.50 (–OCH_2CH_2–, ether groups), 5.91–9.00 (protons of benzene ring in VPTA).

The complete disappearance of 4.50–4.60 ppm (–OH) active hydrogen in (a) proves that –OH in HPEG has been entirely replaced by –COCOOH. Furthermore, 4.80–4.95 ppm in (b) double bond absorption peaks completely disappeared in (c). This reveals that free radical polymerization among AA and HPEZ has happened. From FT-IR and ^{1}H-NMR analysis, it can conclude that synthesized AA-HPEZ has anticipated structure.

3.3. Influence of PAHV dosage on $CaCO_3$ and $CaSO_4$ inhibition

To understand the performance of PAHV, the inhibition ability of PAHV to control calcium deposits was compared with PAA, PESA, and HPMA at identical conditions. The scale inhibition performance of PAHV and several commercial inhibitors to control $CaCO_3$ and $CaSO_4$ precipitations at different concentrations were shown in Figs. 8 and 9.

The data in Fig. 8 indicates the dosage of PAHV has a strong effect on the formation of calcium carbonate precipitation. As can be seen, the scale inhibition efficiency strengthened with the increasing concentration of PAHV. The inhibition efficiency obtained from PAHV at concentration of 8 mg/L is about 92.1%. Under the same experimental conditions, $CaCO_3$ inhibition of PAHV is much better than HPMA, PAA, and PESA on the same concentration. It can be shown that the order of inhibiting the precipitation of $CaCO_3$ from flask tests was PAHV > PAA > PESA > HPMA.

The data in Fig. 9 show the inhibition performance of PAHV, PPA, PESA and HPMA to $CaSO_4$ scale under identical conditions. Compared to the several commercial inhibitors, the PAHV shows superior performance to inhibit $CaSO_4$ scale. It was indicated that the order of preventing the precipitation of $CaSO_4$ was PAHV > PAA > PESA > HPMA, the ultimate inhibition efficiency values were 98.9%, 92.5%, 91.3%, 93.6%, and 86.6% at the threshold dosage of 4 mg/L, respectively.

Molecular structures of PAA, HPMA and PAHV all contain carboxyl groups, but the efficiency of PAA and HPMA to inhibit $CaCO_3$ and $CaSO_4$ scales are poor even at a high dosage. It may be that the side-chain polyethylene (PEG) segments and carboxyl groups of PAHV play an important role during the control of $CaCO_3$ scales [26]. The functional groups of inhibitors exhibit a significant impact on inhibitory power in terms of controlling calcium scales precipitation. Taking Figs. 8 and 9 into account, it can be concluded that the studied inhibitor PAHV can be used as an efficient non-phosphorus scale inhibitor for $CaCO_3$ and $CaSO_4$ in cooling water systems.

3.4. Scale surface morphology characterization

3.4.1. SEM studies

The SEM photographs for collected $CaCO_3$ scale formed in simulative cooling water in the absence and the presence of copolymer are presented in Fig. 10. The SEM image

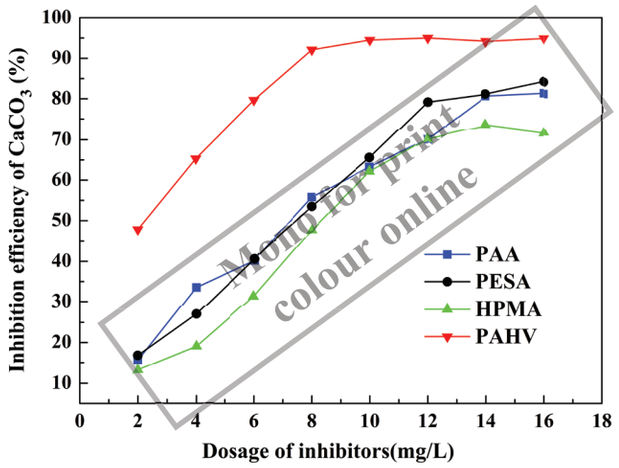

Fig. 8. Comparison of scale inhibition efficiency on $CaCO_3$ of PAHV and different commercial inhibitors.

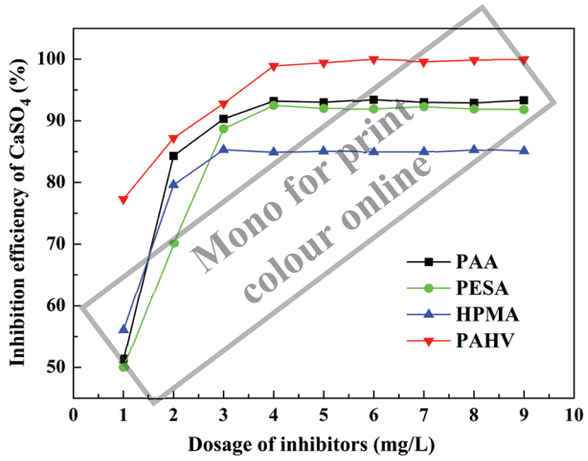

Fig. 9. Comparison of scale inhibition efficiency on $CaSO_4$ of PAHV and different commercial inhibitors.

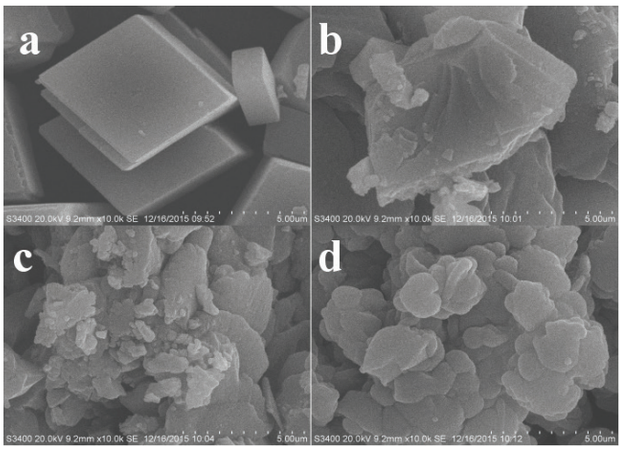

Fig. 10. SEM photographs for the calcium carbonate: without the presence of PAHV (a), with the presence of 2 mg/L (b), 4 mg/L (c), and 6 mg/L (d) PAHV.

without the presence of inhibitor revealed that the formation of $CaCO_3$ crystal was well-regulated cubic octahedral crystal shaped particles (Fig. 10(a)). In contrast, on addition of the additive, sharp edges of the crystals disappeared and became roughened (Figs. 10(b)–(d)), and the formations were porous, amorphous, and irregular. Based on the above analysis, these changes indicate the presence of the additive have a significant impact on the nucleation and morphology of the $CaCO_3$ precipitate. Besides, the crystal shape was changed to form spongy deposits, which can be easily washed away by water flowing.

The SEM images for calcium sulfate precipitate with and without the presence of inhibitors are shown in Fig. 11. Compared with the two photographs, the size and shape of the $CaSO_4$ precipitation were different due to the presence of PAHV. As can be seen from Fig. 11(a) the crystals of $CaSO_4$ are rod-shaped and regular thin tubular cells displaying monoclinic symmetry in the absence of PAHV. However, In the presence of 2 mg/L PAHV (Fig. 11(b)), sharp edges and acute corners of the crystals disappeared almost completely became defective rods.

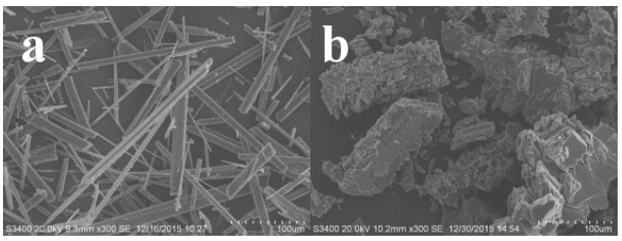

Fig. 11. SEM photographs for the calcium sulfate: without the presence of PAHV (a), with the presence of 2 mg/L PAHV (b).

3.4.2. XRD studies

In order to further researach $CaCO_3$ crystals, the XRD was measured in Fig. 12. It is generally known that $CaCO_3$ have three types of crystal forms: calcite, aragonite, and vaterite [28]. In the absence of the inhibitior, $CaCO_3$ crystallizes as calcite, which is the most thermodynamically stable crystal in Fig. 12(a). This indicated that the crystal of calcium carbonate was mainly an ingredient of calcite. However, both the intense peaks of calcite and vaterite have been observed in Fig. 12(b) on the addition of 4 mg/L of PAHV. According to the analysis between XRD and SEM, PAHV not only can chealte with Ca^{2+}, but also change nucleation and Crystal of $CaCO_3$.

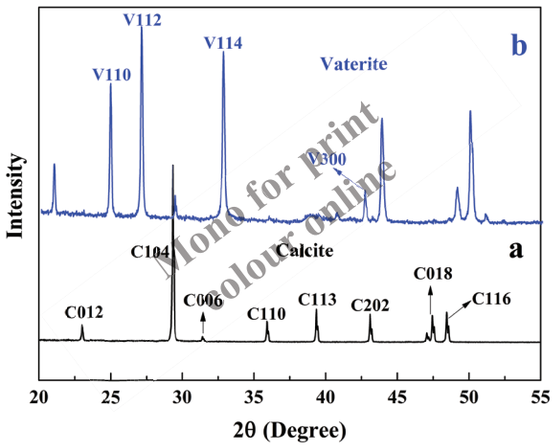

Fig. 12. XRD images of the $CaCO_3$ crystal formed (a) in the absence of PAHV and (b) with the presence of 4 mg/L PAHV.

$CaSO_4$ scales with and without PAHV copolymer were investigated using XRD. As shown in Fig. 13, the interplanar crystal spacing (d) and angle of intersection (Degree) values conformed to the structure of gypsum (calcium sulfate di-hydrate) [29], XRD results showed no modification in the crystal structure and morphology from Fig. 13, but modification of the morphology can be observed from the SEM photographs (Fig. 11(b)).

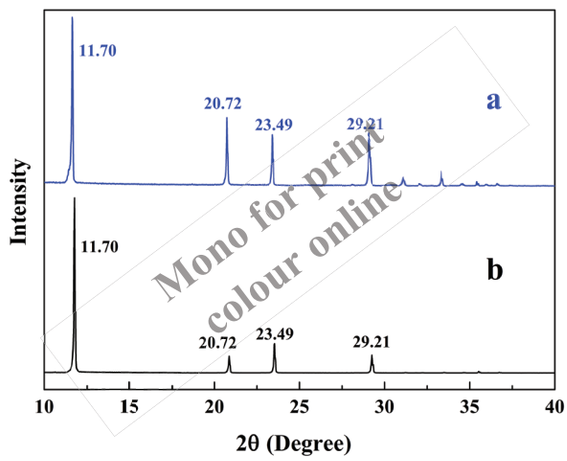

Fig. 13. XRD images of the $CaSO_4$ crystal formed (a) in the absence of PAHV and (b) with the presence of 2 mg/L PAHV.

3.5. The mechanism of calcium scale inhibition

The PAHV's functional groups exhibit a significant influence on the inhibitory power in terms of modifying the structure of calcium scales and crystal morphology. It is likely attributed to the PAHV contains carboxylic acid groups (–COOH) which could interact with mineral nuclei by binding multivalent cation with powerful affinities [30]. Linear polymers like PAA and HPMA which has a long chain carboxyl often lack of secondary and tertiary structures tend to inter-wine with each other [12]. Moreover, the functional groups are not all exposed due to hydrogen bonding between the carboxylic groups. Encapsulation quantity of the metallic ions by the carboxylic groups is erratic because most of them are twisted in the core. However, PAHV shows large extension in water solution on account of steric hindrance and chelate calcium ions. Besides, the sulfonic acid groups increase polymer solubility which makes the molecular chain extension better. The excellent dispersion capability was not only provided by spatial repulsion but also due to the existence of strong hydrogen bonding between the –COOH groups and the water molecules or inter-molecularly. As a result, the sequestration of Ca^{2+} or crystal nucleus becomes more easily. After chelating calcium

ions, –COOH segment of PAHV adsorb onto calcium scales microcrystal particles surface, then the PAHV–Ca complexes could weaken the free calcium ion activity and lower the degree of supersaturation. In addition, with the electrostatic repulsion force increasing between crystallites, the growth of $CaCO_3$ and $CaSO_4$ particles is hindered. Therefore, PAHV could keep the crystal particles dispersed in the solution, prompting them less prone to sedimentation or adsorption onto the equipment surface.

3.6. Excitation and emission properties of VPTA and PAHV

Excitation and emission wavelength of VPTA (a) and PAHV (b) are represented in Fig. 14. As the data presented in Fig. 14, excitation and emission wavelengths of VPTA and PAHV are 402 and 429 nm, respectively. Chromophore of VPTA and PAHV are all pyranine, so PAHV and VPTA have the same excitation and emission wavelengths like pyranine. Excitation spectra and emission spectra of PAHV exhibit great mirror-image relationship as VPTA. It is obvious that the fluorescence intensity of PAHV has significantly enhancement compared with VPTA after radical copolymerization because of the form of hydrogen bond.

The lowest singlet excited states of aromatic carbonyl compounds such as VPTA is (n, π*). The excited state has (n, π*) character in weakly and non-polar hydrogen bonding solvents. However, they show enhanced (π*, π*) character in quite polar hydrogen bonding solvents. (π*, π*) states are the energetically lowest states after copolymerization. The yields of fluorescence grow in quantity in (π*, π*) states than in (n, π*) states [31].

3.7. Response of fluorescent intensity over a range of PAHV

The linearity testing between PAHV copolymer concentration and fluorescence intensity by subtracting the water blank is shown in Fig. 15. The relationship between the fluorescence intensity and the concentration of PAHV is linear in the scope of 1–9 mg/L which is the range of the common dosage of scale inhibitors. The relationship between PAHV concentration and fluorescence intensity exhibit exceptionally linear response (correlation coefficient r = 0.9971). This excellent linear relationship can be applied to quantitatively measure the concentration of PAHV in cooling water. The detection limit of PAHV is 0.68 mg/L according to the formula: Dr = 3σ/k, where σ is 11 times fluorescence intensity determination of distilled water and k is slope of calibration curve [32].

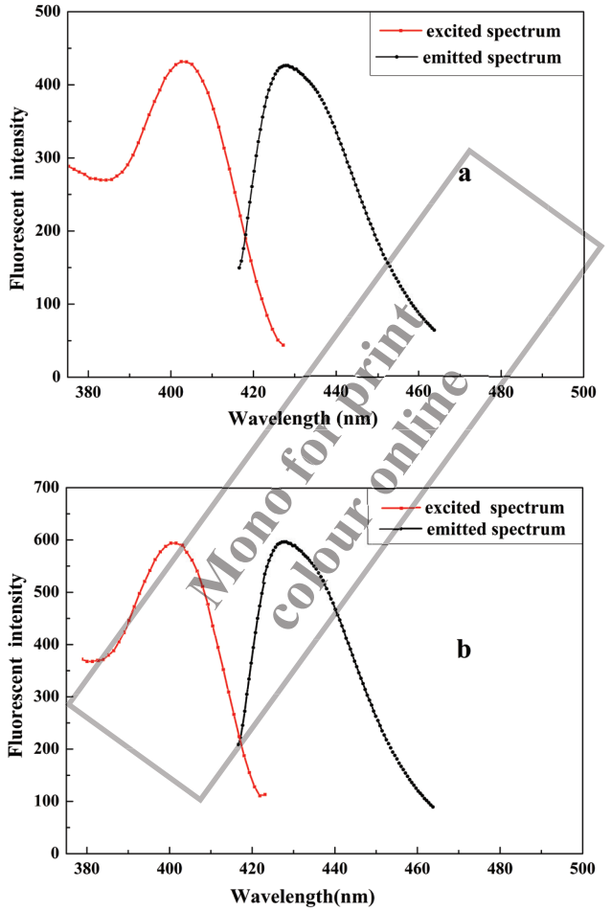

Fig. 14. Excitation and emission wavelength of VPTA (a) and PAHV (b).

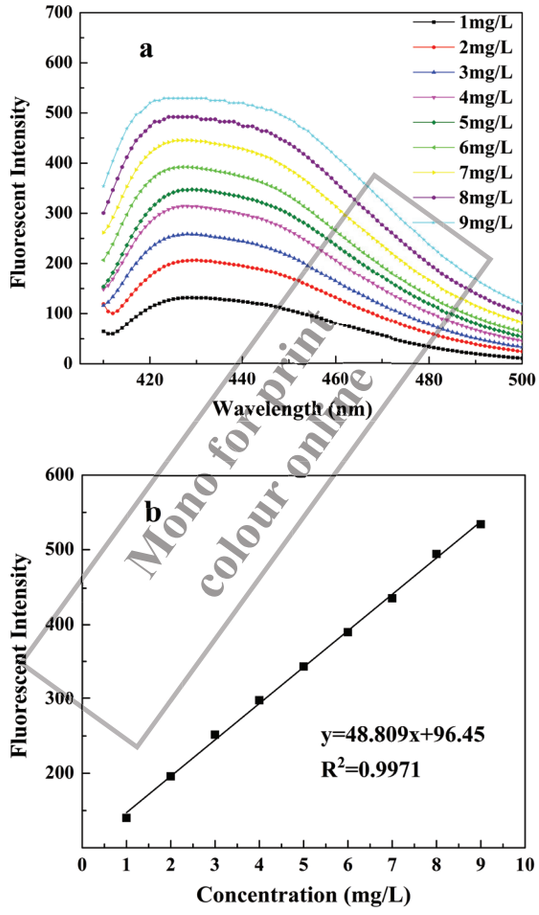

Fig. 15. Correlation of fluorescent intensity and concentration of PAHV.

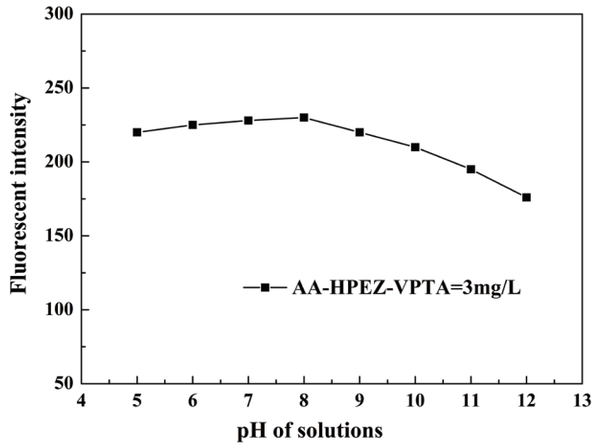

Fig. 16. Relationship between fluorescent intensity and pH of PAHV solutions.

3.8. Effect of pH on scale inhibitor fluorescent intensity

The effects of pH on fluorescent intensity are shown in Fig. 16. As seen in Fig. 16, the fluorescent intensity of PAHV solutions exhibit acceptable volatility at different pH environment. Such results reveal that the linear relationship between fluorescence intensity and concentration can be maintained in the pH range from 5 to 9, a usual value for industrial cooling water systems. Thus, it can be suggested that when PAHV is used in industrial recirculated cooling water systems, the fluorescence intensity and emission band position will scarcely change under normal routine operations. The fluorescence intensity of solutions almost keep steady even the pH (5–9) value changed, this result perhaps owing to the structure of PAHV contains benzene ring [33].

4. Conclusions

The fluorescence scale inhibitior PAHV was synthesized successfully by radical polymerization. Based on the present study, the most important conclusions are summarized below:

- The fluorescent-tagged inhibitor showed 92.1% $CaCO_3$ inhibition at a threshold dosage of 8 mg/L, while it exhibited 98.9% $CaSO_4$ inhibition at a level of 4 mg/L.
- The studies on calcium crystals with SEM and XRD showed that significant changes of the crystal shape, morphology of the calcium scales took place in the presence of PAHV.
- Excellent linear relationship between fluorescent intensity and polymer concentration (the correlation coefficient $r = 0.9971$) guarantees that PAHV possesses a great fluorescent tracer function for cooling water systems.

The pH (value from 5 to 9) of solutions has scarcely influence on the linear relationship between fluorescence intensity and concentration. The concentration of agent can be accurately measured under normal pH value. These results indicate that PAHV can be used as an effective fluorescent-tagged scales inhibitor for industrial cooling water system.

Acknowledgments

This work was supported by a Project Funded by the Priority Academic Program Development of Jiangsu Higher Education Institutions (PAPD); The Fundamental Research Funds for the Central Universities (3207046302); Fund Project for Transformation of Scientific and Technological Achievements of Jiangsu Province of China (BA2014100); and Based on Teachers' scientific research SRTP of southeast University (T16192003).

References

[1] Z. Shen, J. Li, K. Xu, L. Ding, H. Ren, The effect of synthesized hydrolyzed polymaleic anhydride (HPMA) on the crystal of calcium carbonate, Desalination, 284 (2012) 238–244.
[2] R. MacDonald, V.S. Brozel, Community analysis of bacterial biofilms in a simulated recirculating cooling-water system by fluorescent in situ hybridization with rRNA-targeted oligonucleotide probes, Water Res., 34 (2000) 2439–2446.
[3] H.C. Wang, Y.M. Zhou, Q.Z. Yao, W. Sun, Calcium sulfate precipitation studies with fluorescent-tagged scale inhibitor for cooling water systems, Polym. Bull., 72 (2015) 2171–2188.
[4] S. Ghizellaoui, M. Euvrard, Assessing the effect of zinc on the crystallization of calcium carbonate, Desalination, 220 (2008) 394–402.
[5] E. López-Sandoval, C. Vázquez-López, B.E. Zendejas-Leal, G. Ramos, E. San Martín-Martínez, N. Muñoz Aguirre, E. Reguera, Calcium carbonate scale inhibition using the "allotropic cell" device, Desalination, 217 (2007) 85–92.
[6] H.K.Ü. Can, Gizem, Water-soluble anhydride containing alternating copolymers as scale inhibitors, Desalination, 355 (2015) 225–232.
[7] Q. Huang, W. Ma, A model of estimating scaling potential in reverse osmosis and nanofiltration systems, Desalination, 288 (2012) 40–46.
[8] G. Liu, J. Huang, Y. Zhou, Q. Yao, H. Wang, L. Ling, P. Zhang, K. Cao, Y. Liu, W. Wu, W. Sun, Carboxylate-terminated double-hydrophilic block copolymer containing fluorescent groups: an effective and environmentally friendly inhibitor for calcium carbonate scales, Int. J. Polym. Mater., 62 (2013) 678–685.
[9] R. Ketrane, B. Saidani, O. Gil, L. Leleyter, F. Baraud, Efficiency of five scale inhibitors on calcium carbonate precipitation from hard water: effect of temperature and concentration, Desalination, 249 (2009) 1397–1404.
[10] M.M. Reddy, A.R. Hoch, Calcite crystal growth rate inhibition by polycarboxylic acids, J. Colloid Interface Sci., 235 (2001) 365–370.
[11] X. Yin, W. Yang, Y. Tang, Y. Liu, J. Wang, The synergistic effect of orthophosphate and polymer on the precipitation of calcium carbonate, Desalination, 255 (2010) 143–147.
[12] Y.M. Al-Roomi, K.F. Hussain, Application and evaluation of novel acrylic based $CaSO_4$ inhibitors for pipes, Desalination, 355 (2015) 33–44.
[13] X.Y. Sun, J.P. Zhang, C.X. Yin, J.T. Zhang, J. Han, Poly(aspartic acid)-tryptophan grafted copolymer and its scale-inhibition performance, J. Appl. Polym. Sci., 132 (2015) 427,39–42,747.
[14] Y. Liu, C. Zou, C. Li, L. Lin, W. Chen, Evaluation of β-cyclodextrin–polyethylene glycol as green scale inhibitors for produced-water in shale gas well, Desalination, 377 (2016) 28–33.
[15] D.Y. Li, Y.P. Qin, H.Y. Li, X.W. He, W.Y. Li, Y.K. Zhang, A "turn-on" fluorescent receptor for detecting tyrosine phosphopeptide using the surface imprinting procedure and the epitope approach, Biosens. Bioelectron., 66 (2015) 224–230.
[16] A. Balamurugan, H.-I. Lee, Water-soluble polymeric probes for the selective sensing of mercury ion: pH-driven controllable detection sensitivity and time, Macromolecules, 48 (2015) 1048–1054.

[17] J. Hu, L. Dai, S. Liu, Analyte-reactive amphiphilic thermoresponsive diblock copolymer micelles-based multifunctional ratiometric fluorescent chemosensors, Macromolecules, 44 (2011) 4699–4710.
[18] J. Kollár, P. Hrdlovič, Š. Chmela, Spectral properties of bichromophoric pyrene derivatives: monomer vs. excimer fluorescence, J. Photochem. Photobiol. A, 214 (2010) 33–39.
[19] P. Chandar, P. Somasundaran, N.J. Turro, Fluorescence probe investigation of anionic polymer cationic surfactant interactions, Macromolecules, 21 (1988) 950–953.
[20] B.E. Moriarty, J.E. Hoots, D.P. Workman, J.P. Rasimas, Fluorescent monomers and polymers containing same for use in industrial water systems, US Patent, (2001) 6312644.
[21] Y. Li, C. Yang, Y. Zhang, J. Zheng, H. Guo, M. Lu, Study on dispersion, adsorption and flow retaining behaviors of cement mortars with TPEG-type polyether kind polycarboxylate superplasticizers, Construction Building Mater., 64 (2014) 324–332.
[22] Y. Liu, Y. Zhou, Q. Yao, W. Sun, Evaluating the performance of PEG-based scale inhibition and dispersion agent in cooling water systems, Desal. Wat. Treat., 56 (2014) 1309–1320.
[23] Y. Chen, Y. Zhou, Q. Yao, Y. Bu, H. Wang, W. Wu, W. Sun, Evaluation of a low-phosphorus terpolymer as calcium scales inhibitor in cooling water, Desal. Wat. Treat., 55 (2014) 945–955.
[24] Y. Bu, Y. Zhou, Q. Yao, Y. Chen, W. Sun, W. Wu, Inhibition of calcium carbonate and sulfate scales by a non-phosphorus terpolymer AA-APEY-AMPS, Desal. Wat. Treat., 57 (2014) 1977–1987.
[25] H. Wang, Y. Zhou, G. Liu, J. Huang, Q. Yao, S. Ma, K. Cao, Y. Liu, W. Wu, W. Sun, Z. Hu, Investigation of calcium carbonate precipitation in the presence of fluorescent-tagged scale inhibitor for cooling water systems, Desal. Wat. Treat., 53 (2013) 3491–3498.
[26] F. Change, Z. Yuming, L. Guangqing, H. Jingyi, S. Wei, W. Wendao, Inhibition of $Ca_3(PO_4)_2$, $CaCO_3$, and $CaSO_4$ precipitation for industrial recycling water, Ind. Eng. Chem. Res., 50 (2011) 10393–10399.
[27] H. Wang, Y. Zhou, Q. Yao, S. Ma, W. Wu, W. Sun, Synthesis of fluorescent-tagged scale inhibitor and evaluation of its calcium carbonate precipitation performance, Desalination, 340 (2014) 1–10.
[28] G. Nehrke, P. Van Cappellen, Framboidal vaterite aggregates and their transformation into calcite: a morphological study, J. Cryst. Growth, 287 (2006) 528–530.
[29] X. Mao, X. Song, G. Lu, Y. Xu, Y. Sun, J. Yu, Effect of additives on the morphology of calcium sulfate hemihydrate: experimental and molecular dynamics simulation studies, Chem. Eng. J., 278 (2015) 320–327.
[30] M. Pons-Jiménez, R. Hernández-Altamirano, R. Cisneros-Dévora, E. Buenrostro-González, R. Oviedo-Roa, J.-M. Martínez-Magadán, L.S. Zamudio-Rivera, Theoretical and experimental insights into the control of calcium sulfate scales by using random copolymers based on itaconic acid, Fuel, 149 (2015) 66–77.
[31] R. Rusakowi, G.W. Byers, P.A. Leermake, Electronically excited aromatic carbonyl compounds in hydrogen bonding and acidic media, J. Am. Chem. Soc., 93 (1971) 3263–3266.
[32] L.J. Gao, J.Y. Feng, B. Jin, Q.N. Zhang, T.Q. Liu, Y.Q. Lun, Z.J. Wu, Carbazole and Hydroxy Groups-tagged Poly(aspartic acid) scale inhibitor for cooling water systems, Chem. Lett., 40 (2011) 1392–1394.
[33] D. Li, C.Y. Li, H.R. Qi, K.Y. Tan, Y.F. Li, Rhodamine-based chemosensor for fluorescence determination of trivalent chromium ion in living cells, Sens. Actuators B, 223 (2016) 705–712.